



Humanoids

Multimodal sensing and self-calibration

Doc. Mgr. Matěj Hoffmann, Ph.D.

Department of Cybernetics, Faculty of Electrical Engineering

Czech Technical University in Prague

matej.hoffmann@fel.cvut.cz

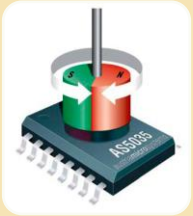
<https://sites.google.com/site/matejhof>

<https://cyber.felk.cvut.cz/research/groups-teams/humanoids/>



Sensors in a robot manipulator - position

- Encoders



Position Sensors

- 45 Absolute Position Sensors in the joints (analog or digital hall effect sensor) (12 bits/turn)
- 20 optical encoders for DC motors (10 to 12 bits/turn)
- 11 Reflective Encoder on the ROTOR shaft of the BLDC Motors (about 12 bits/turn)

Marco Maggiali, iCub system architecture 2021

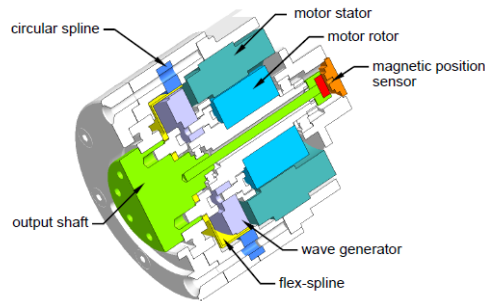
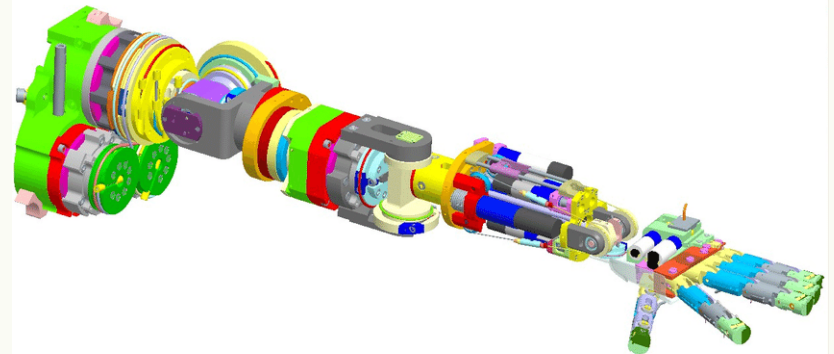


Fig. 3. Motor group cross section. The figure shows a cross section of a iCub motor group. The Harmonic-Drive and Kollmorgen brushless motor are clearly visible.

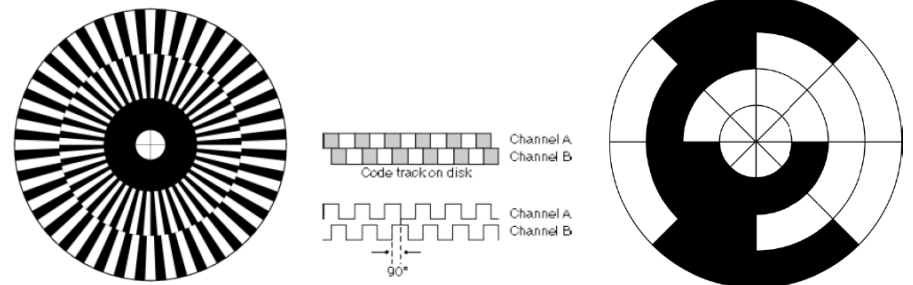


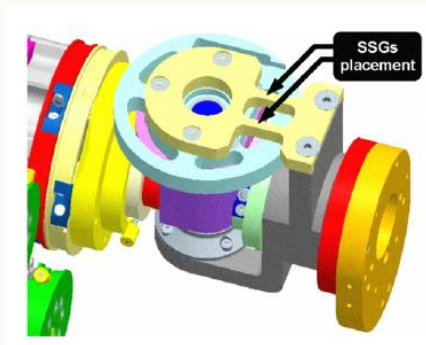
Figure 7.2. From left to right: encoder pattern used in a quadrature encoder, resulting sensor signal (forward motion), absolute encoder pattern (gray coding).

Correll, N., Hayes, B., Heckman, C., Roncone, A. (2022).

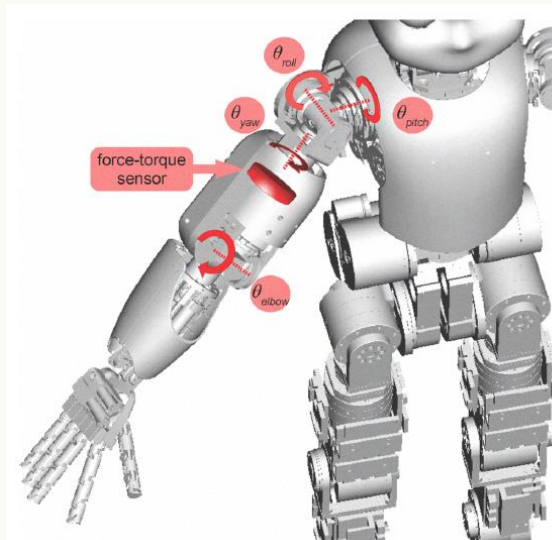
- What is it enough for?

Sensors in a manipulator – force / torque

- motor current – motor load
 - with complex modeling, joint torques and possibly ext. wrenches can be *coarsely* estimated
- force/torque sensor at the flange
- joint torque sensors
- force/torque sensor located proximally

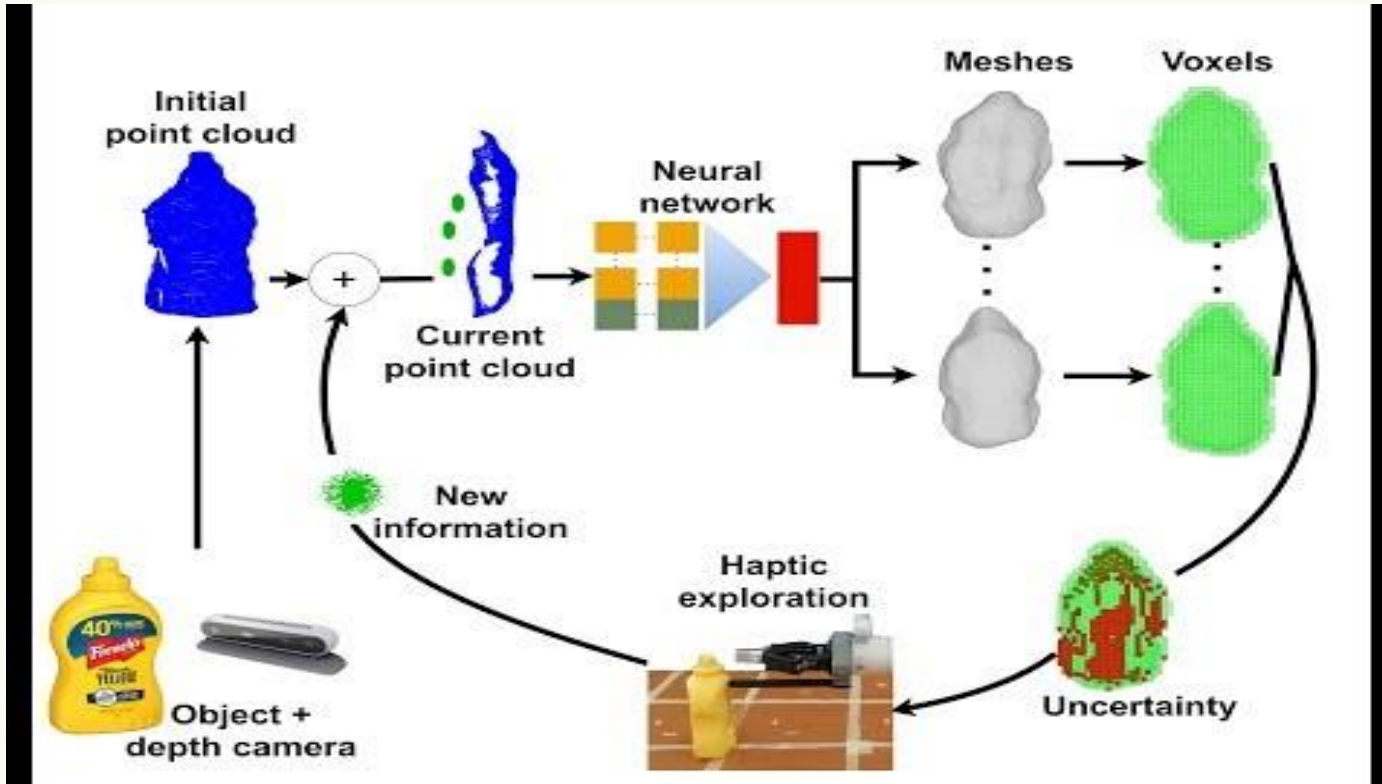


shoulder roll with semiconductor strain gauge



Discussion

Example – contact detection



From 1:10 in
<https://youtu.be/iZF4ph4zMEA>

Rustler, L., Lundell, J., Behrens, J. K., Kyrki, V., & Hoffmann, M. (2022). 'Active Visuo-Haptic Object Shape Completion'. *IEEE Robotics and Automation Letters* 7 (2), 5254-5261.

External torque estimation



● joint torque sensors

$$\boldsymbol{\tau} = \boldsymbol{M}(\boldsymbol{q})\ddot{\boldsymbol{q}} + \boldsymbol{C}(\boldsymbol{q}, \dot{\boldsymbol{q}})\dot{\boldsymbol{q}} + \boldsymbol{g}(\boldsymbol{q}) + \boldsymbol{\tau}_F + \boldsymbol{\tau}_{ext} = \boldsymbol{\tau}_{dyn} + \boldsymbol{\tau}_{ext}$$

$\boldsymbol{M}(\boldsymbol{q}) \in \mathbb{R}^{n \times n}$ joint space inertia matrix

$\boldsymbol{C}(\boldsymbol{q}, \dot{\boldsymbol{q}})\dot{\boldsymbol{q}} \in \mathbb{R}^n$ centripetal and Coriolis vector

$\boldsymbol{g}(\boldsymbol{q}) \in \mathbb{R}^n$ gravity vector

$\boldsymbol{\tau} \in \mathbb{R}^n$ joint torque measured by sensor

$\boldsymbol{\tau}_{dyn} \in \mathbb{R}^n$ torque computed from dynamics

- results from the configuration, velocity and acceleration of the robot
- can be obtained with dynamics simulator (e.g. OpenRave)

$\boldsymbol{\tau}_F \in \mathbb{R}^n$ dissipative friction torque

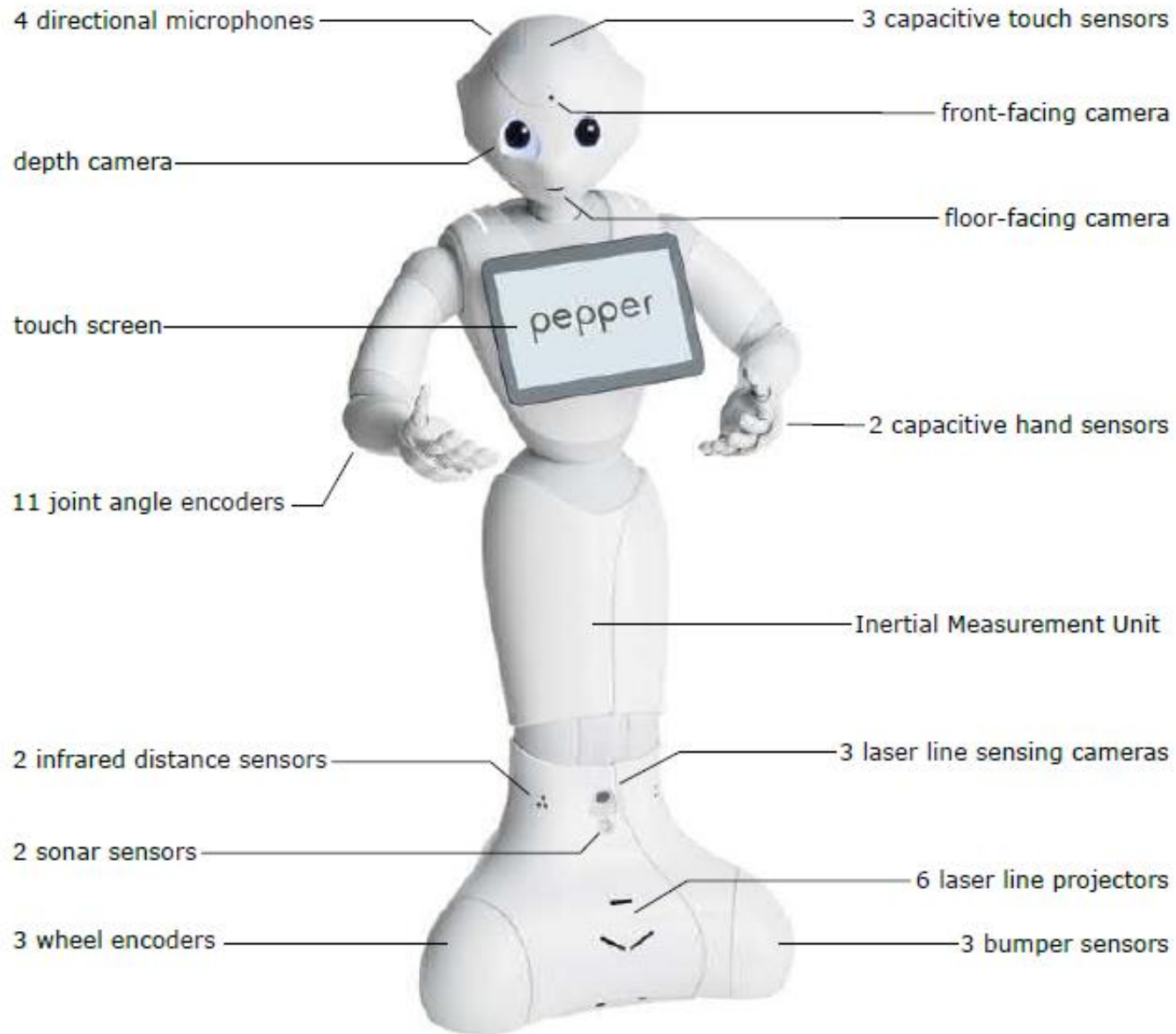
$\boldsymbol{\tau}_{ext} \in \mathbb{R}^n$ external joint torque ($\boldsymbol{\tau}_{ext} = \boldsymbol{J}^T(\boldsymbol{q})\boldsymbol{F}_{ext}$)

$$\boldsymbol{\tau}_{ext} = \boldsymbol{\tau} - \boldsymbol{\tau}_{dyn}$$

Humanoids have much more than that ...

- 53+ joint encoders
- 4 F/T sensors
- 2 cameras
- tactile sensors
 - cca 4000 pressure-sensitive tactile elements (taxels) on the whole body
- inertial sensors
- microphones...





Why do we need all that?

- To make the robot look more like a human?
- No. Much less is needed for that.



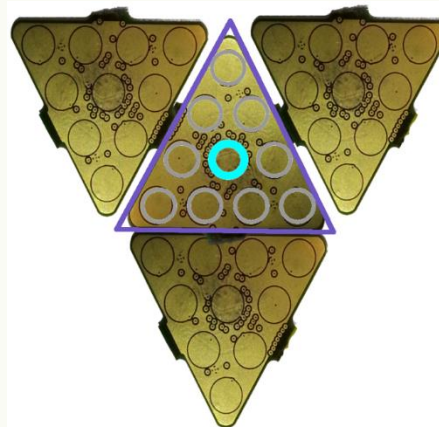
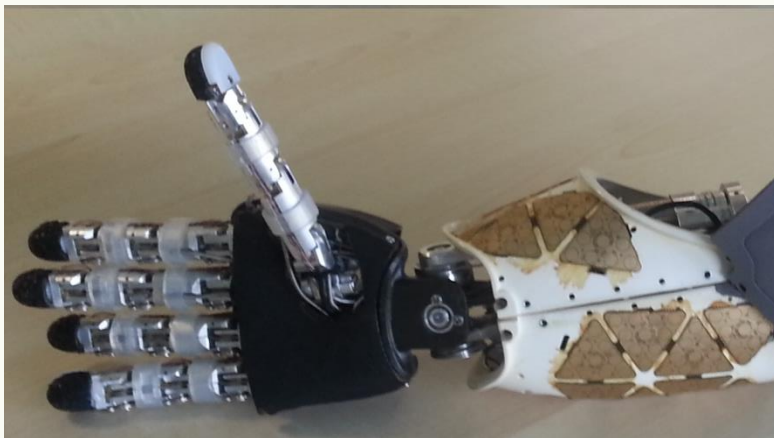
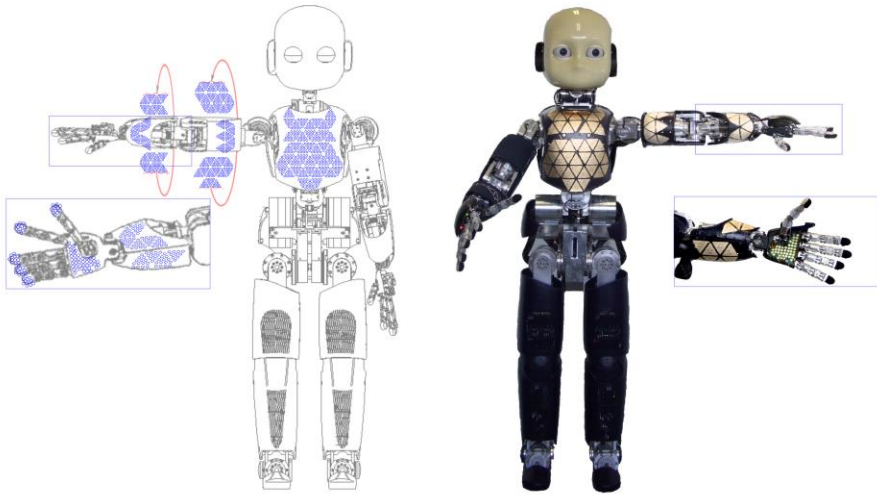
Keepon by Hideki Kozima

Robots with electronic skin

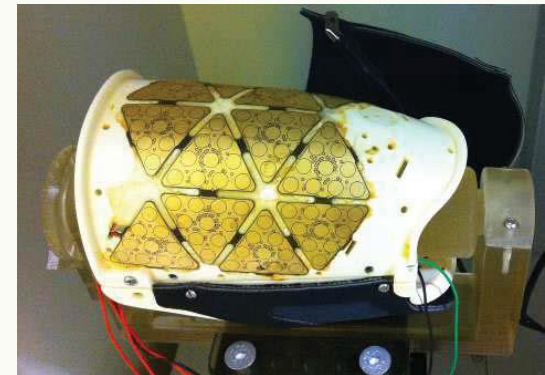
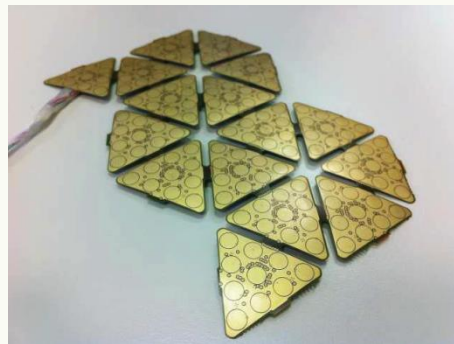
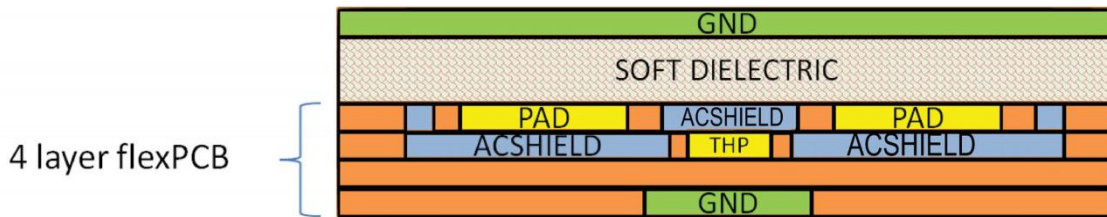
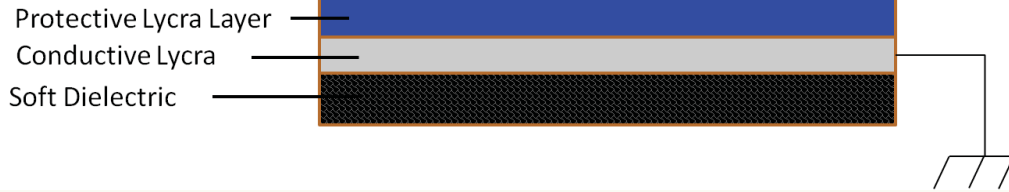
- It seems quite clear why cameras or microphones are useful...
- Why skin?
 - Whole-body contact sensing and regulation
 - For HRI:
 - Safety
 - Contact detection and localization
 - Skin on whole body => safety of whole body
 - Social interaction



Humanoids with artificial skin



The capacitive robot skin



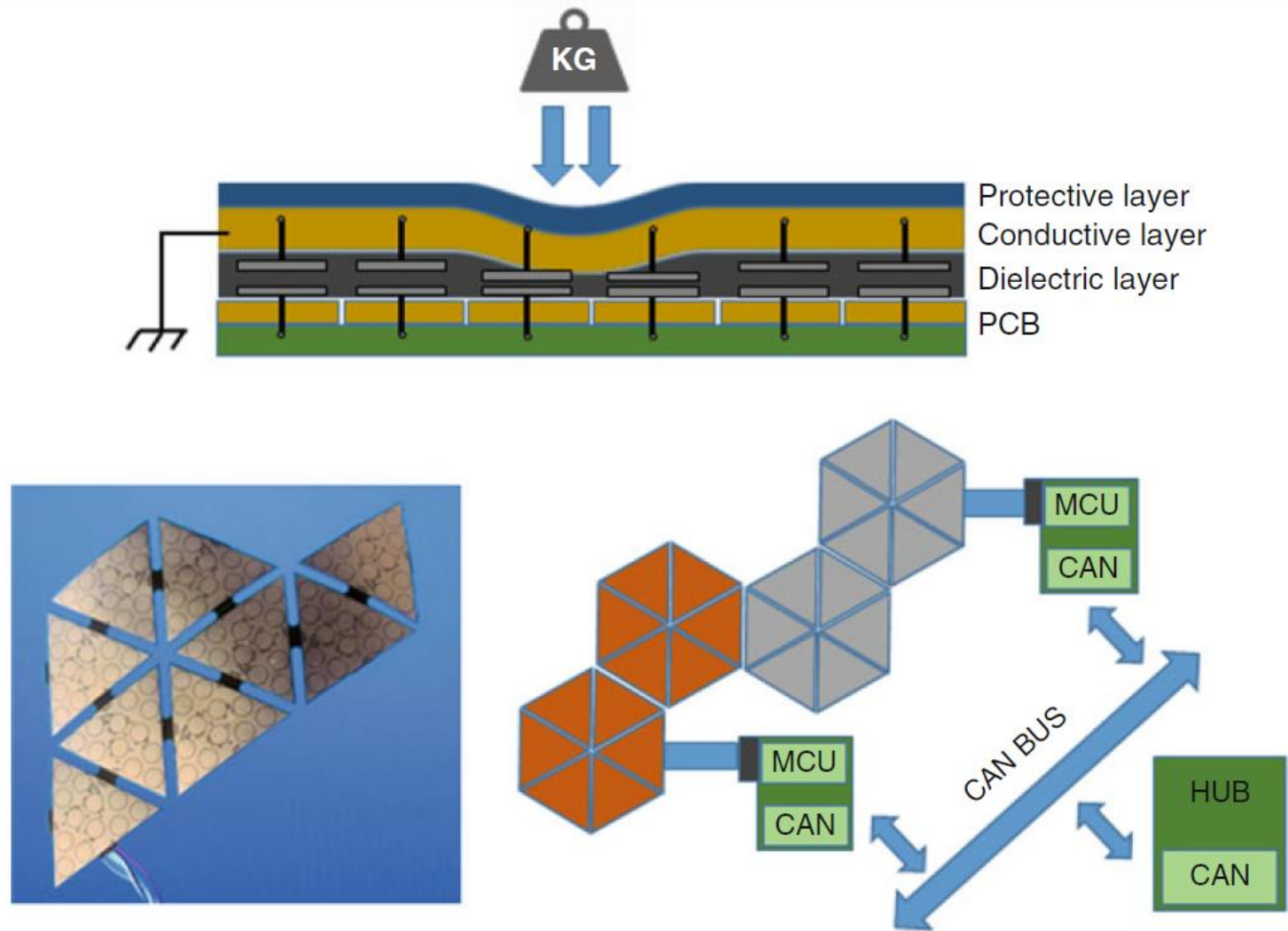


Fig. 8 The iCub skin. *Top*: a schematic representation of the three layers that form the set of capacitors each providing pressure information. *Bottom*: details of the triangular elements and how they are interconnected to form a mesh of sensors that can be read using CAN bus interface

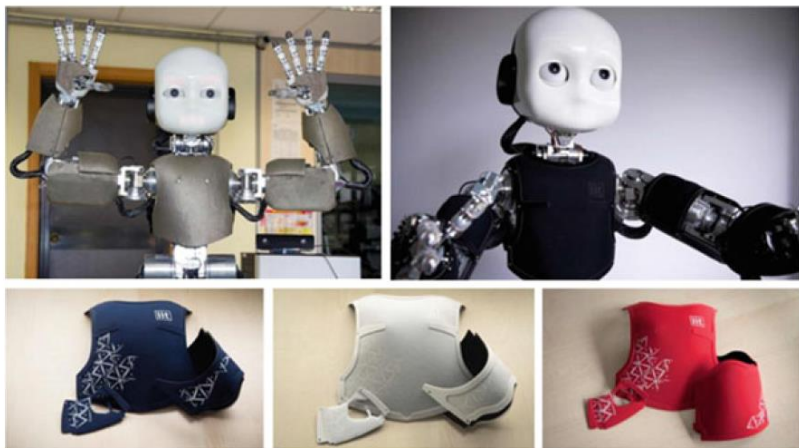
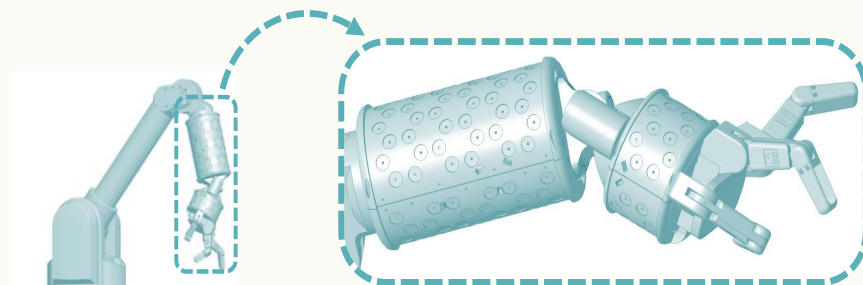


Fig. 9 The first version of the skin used a silicone layered as dielectric, covered with conductive Lycra (*top left*). In the second version of the skin, these layers were replaced by a sandwich of three layers made of fabrics glued with industrial techniques. Among the advantages of this solution is the fact that the production of the fabric is automated and more reliable. The picture on the *top right* shows the latest version of the skin. The figures on the *bottom* show possible customizations in different colors

Natale, L., Bartolozzi, C., Nori, F., Sandini, G., & Metta, G. (2019). iCub. In Goswami, A., & Vadakkepat, P. (Eds.): Humanoid robotics: A reference. Springer. pp. 291-323.



Maiolino, P.; Maggiali, M.; Cannata, G.; Metta, G. & Natale, L. (2013), 'A flexible and robust large scale capacitive tactile system for robots', *Sensors Journal, IEEE 13(10)*, 3910--3917.

Collaborative robots with protective skin



Inertial measurement unit

- What is it?
 - 3-axis accelerometer, 3x gyroscope, magnetometer (~ compass)
 - what use is it for a humanoid robot?
 - where would you place it?

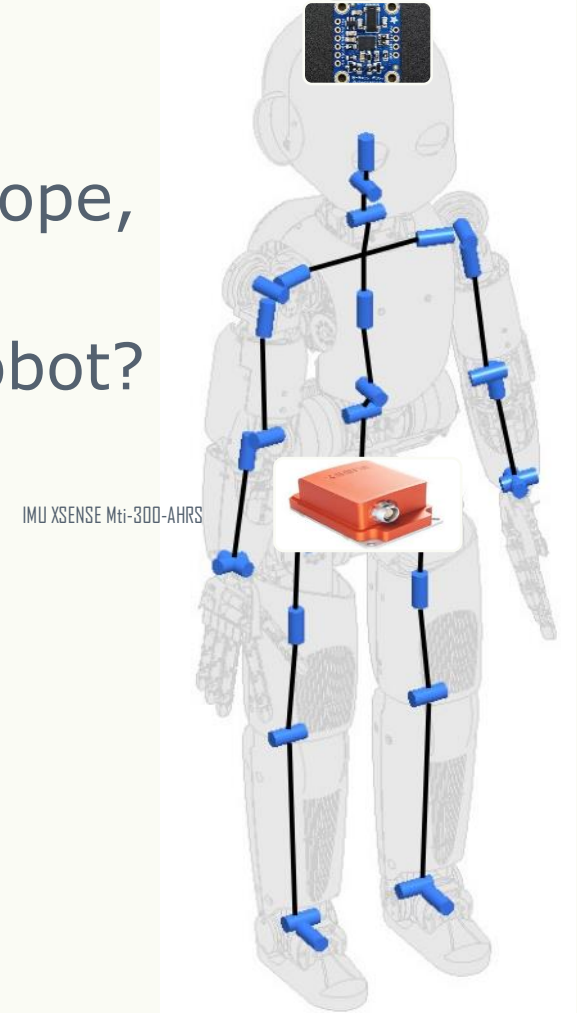


Table 5.1 Classification of sensors frequently used in robotics according to sensing objective (proprioception (PC)/exteroception (EC)) and method (active/passive)

Classification	Sensor type	Sens	A/P
Tactile sensors	Switches/bumpers	EC	P
	Optical barriers	EC	A
	Proximity	EC	P/A
Haptic sensors	Contact arrays	EC	P
	Force/torque	PC/EC	P
	Resistive	EC	P
Motor/axis sensors	Brush encoders	PC	P
	Potentiometers	PC	P
	Resolvers	PC	A
	Optical encoders	PC	A
	Magnetic encoders	PC	A
	Inductive encoders	PC	A
	Capacity encoders	EC	A
Heading sensors	Compass	EC	P
	Gyroscopes	PC	P
	Inclinometers	EC	A/P
Beacon based (position wrt an inertial frame)	GPS	EC	A
	Active optical	EC	A
	Radio frequency (RF) beacons	EC	A
	Ultrasound beacon	EC	A
	Reflective beacons	EC	A
Ranging	Capacitive sensor	EC	P
	Magnetic sensors	EC	P/A
	Camera	EC	P/A
	Sonar	EC	A
	Laser range	EC	A
	Structured light	EC	A
Speed/motion	Doppler radar	EC	A
	Doppler sound	EC	A
	Camera	EC	P
	Accelerometer	EC	P
Identification	Camera	EC	P
	Radio frequency identification RFID	EC	A
	Laser ranging	EC	A
	Radar	EC	A
	Ultrasound	EC	A
	Sound	EC	P

Christensen, H. I., & Hager, G. D. (2016). Sensing and estimation. In *Springer Handbook of Robotics* (pp. 91-112). Springer, Cham.

Redundant and inaccurate sensory information

- Engineer's dream: 1 quantity to be measured \sim 1 sensor with perfect accuracy
- Biological reality: large number of inaccurate signals with nonlinear relationships to the measured quantity
- Example: proprioception

Muscle and skeletal mechanoreceptors

Receptor	Fiber group / name	Submodality
Muscle spindle primary	$A\alpha/Ia$	Muscle length and speed
Muscle spindle secondary	$A\beta/II$	Muscle stretch (\sim length)
Golgi tendon organ	$A\alpha/Ib$	Muscle contraction / tension (\sim force)
Joint capsule mechanoreceptors	$A\beta/II$	Joint angle

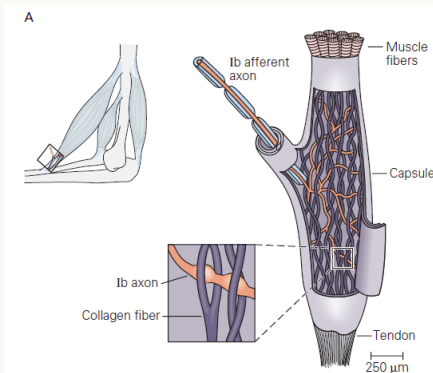
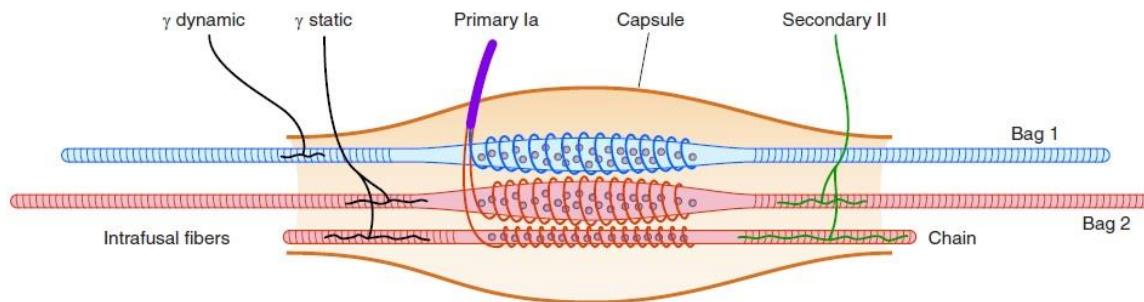
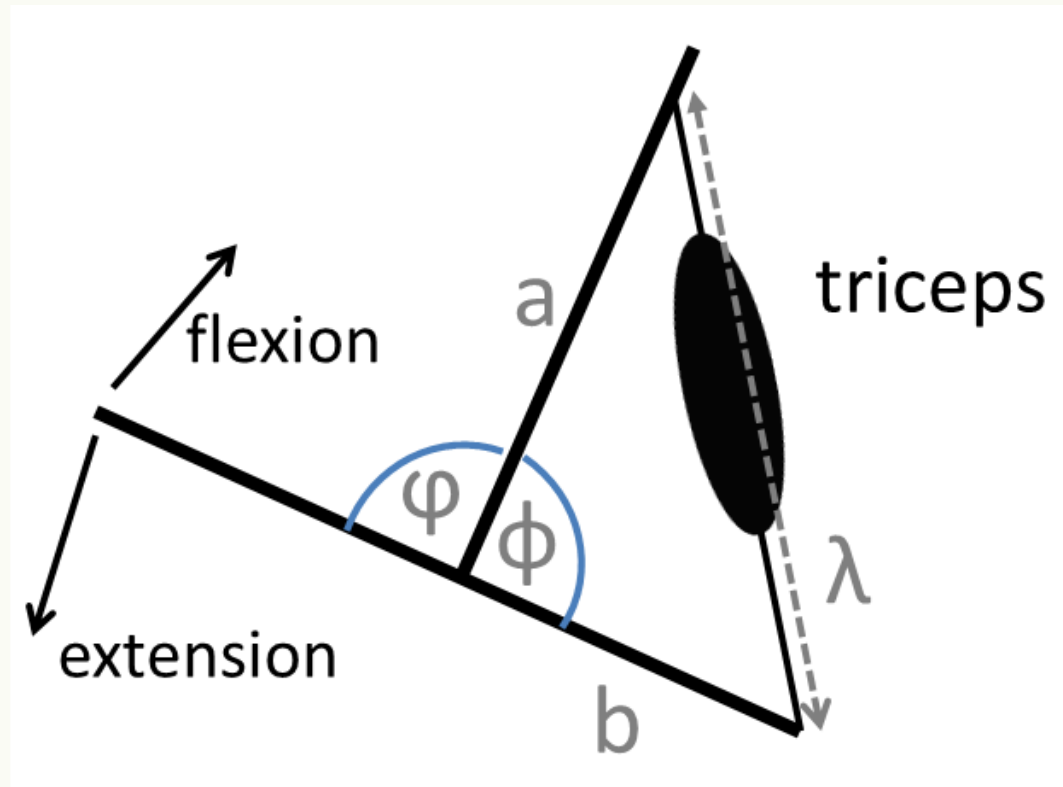


Figure 32-7A When the Golgi tendon organ is stretched (usually because of contraction of the muscle), the Ib afferent axon is compressed by collagen fibers (see enlargement) and its rate of firing increases. (Adapted, with permission, from Schmidt 1983; inset adapted, with permission, from Swett and Scholtz 1975.)

Kandel, E. R. et al. (2021). *Principles of neural science, 6th edition*. New York: McGraw-hill.

From muscle length to joint angle



$$\lambda = \sqrt{a^2 + b^2 - 2 \cdot a \cdot b \cdot \cos(\theta)}$$

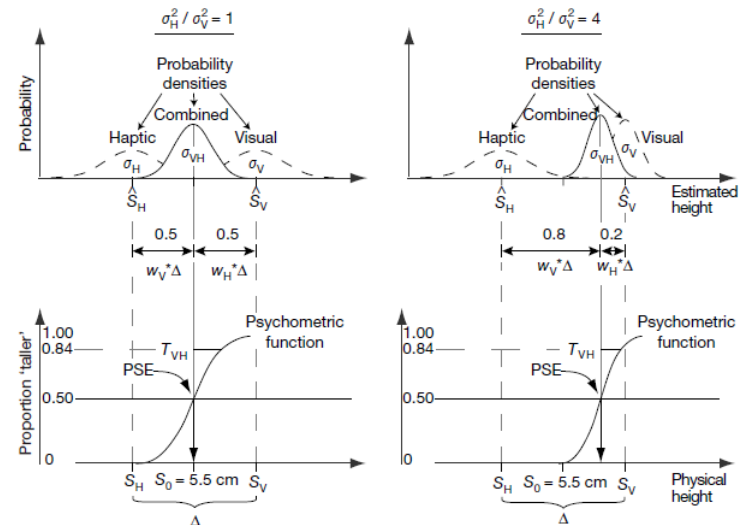
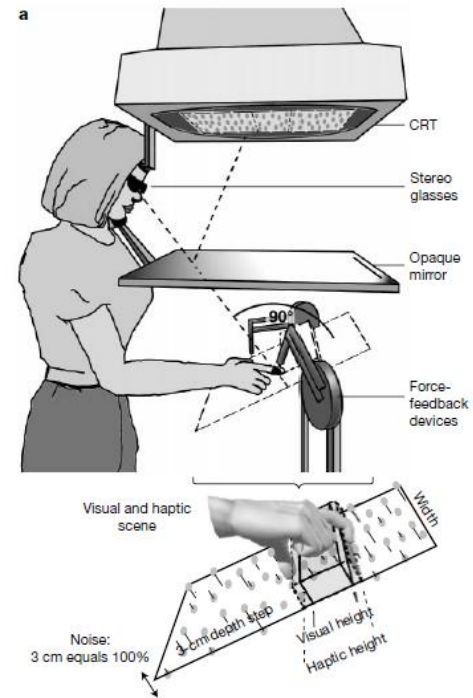
Redundancy is key to learning

Humans integrate visual and haptic information in a statistically optimal fashion

Marc O. Ernst* & Martin S. Banks

Vision Science Program/School of Optometry, University of California, Berkeley
94720-2020, USA

When a person looks at an object while exploring it with their hand, vision and touch both provide information for estimating the properties of the object. Vision frequently dominates the integrated visual-haptic percept, for example when judging size, shape or position¹⁻³, but in some circumstances the percept is clearly affected by haptics⁴⁻⁷. Here we propose that a general principle, which minimizes variance in the final estimate, determines the degree to which vision or haptics dominates. This principle is realized by using maximum-likelihood estimation⁸⁻¹⁵ to combine the inputs. To investigate cue combination quantitatively, we first measured the variances associated with visual and haptic estimation of height. We then used these measurements to construct a maximum-likelihood integrator. This model behaved very similarly to humans in a visual-haptic task. Thus, the nervous system seems to combine visual and haptic information in a fashion that is similar to a maximum-likelihood integrator. Visual dominance occurs when the variance associated with visual estimation is lower than that associated with haptic estimation.

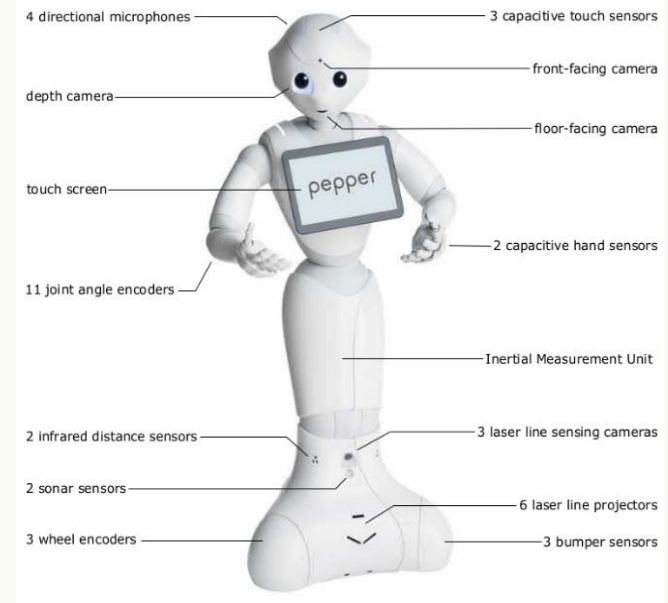


Automatic self-contained robot calibration - motivation

Traditional calibration procedures:
external measuring apparatus ->
impractical when frequent changes
(robot, site where deployed)

Current robots:

- cheaper and more elastic materials
- set of affordable but increasingly accurate sensors (e.g. RGB-D cameras, tactile, force, or inertial sensors, etc.)



Motivation

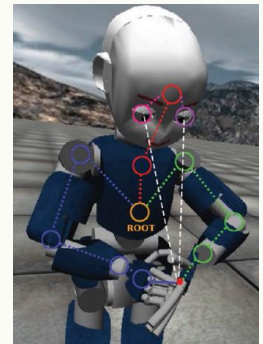
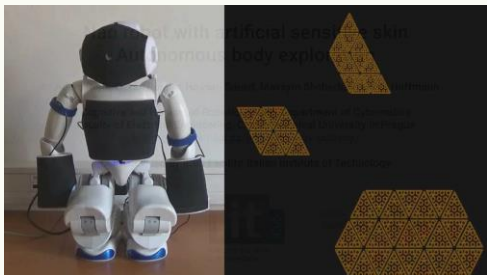
Traditional calibration approaches:

- open-loop (external metrology)
- closed-loop (in contact with the environment)

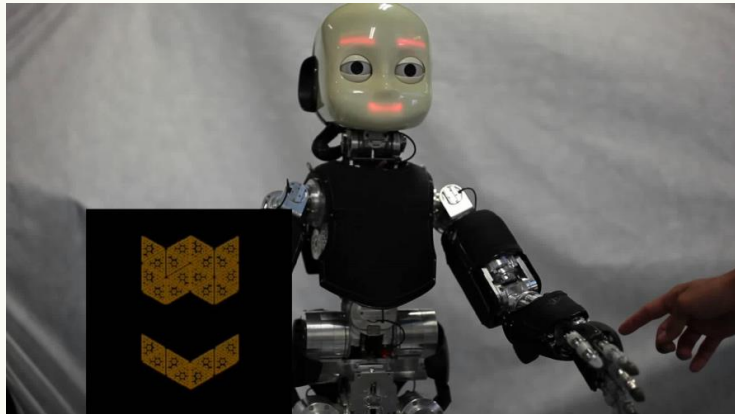


- + camera reprojection errors
- + constraints arising from robot self-contact
- + simultaneous calibration of multiple kinematic chains

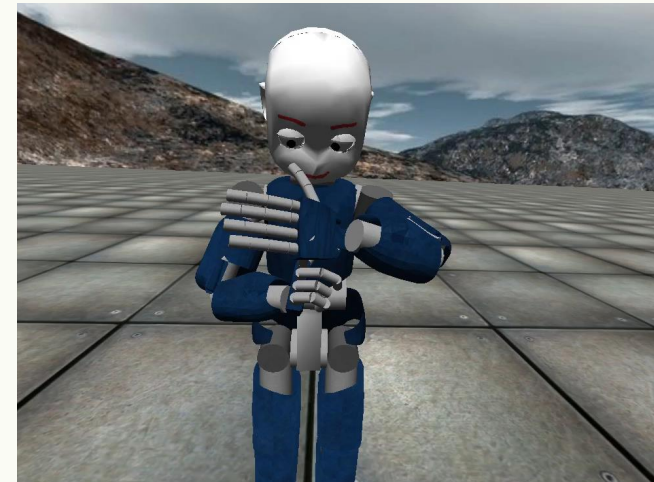
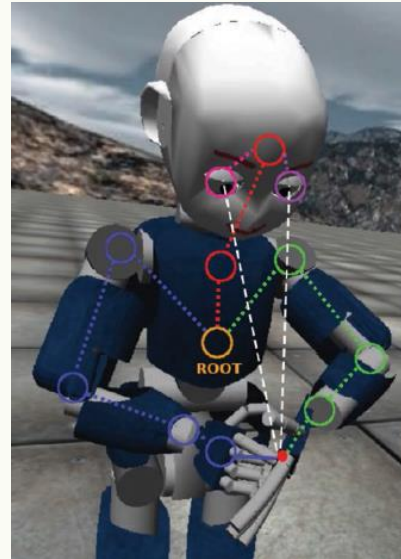
**automatic self-contained robot
calibration**



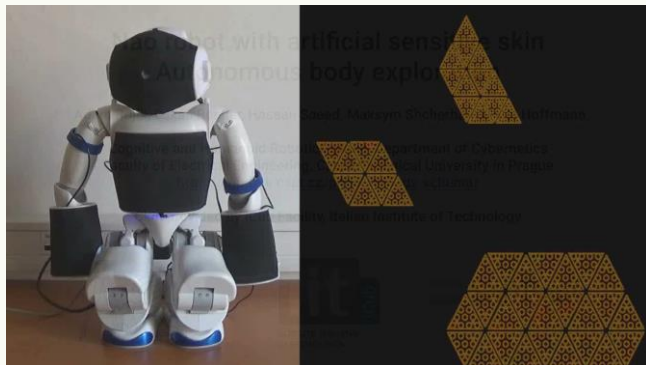
Multisensorial self-contained robot calibration



Roncone, A.; Hoffmann, M.; Pattacini, U. & Metta, G. (2014), Automatic kinematic chain calibration using artificial skin: self-touch in the iCub humanoid robot, in 'Proc. IEEE Int. Conf. Robotics and Automation (ICRA)'.



Stepanova, K.; Pajdla, T. & Hoffmann, M. (2019), 'Robot self-calibration using multiple kinematic chains – a simulation study on the iCub humanoid robot', *IEEE Robotics and Automation Letters* **4**(2), 1900-1907.



Rustler, L.; Potocna, B.; Polic, M.; Stepanova, K. & Hoffmann, M. (2021), Spatial calibration of whole-body artificial skin on a humanoid robot: comparing self-contact, 3D reconstruction, and CAD-based calibration, in 'Humanoid Robots (Humanoids), IEEE-RAS International Conference on'.

<https://github.com/ctu-vras/multirobot-calibration>



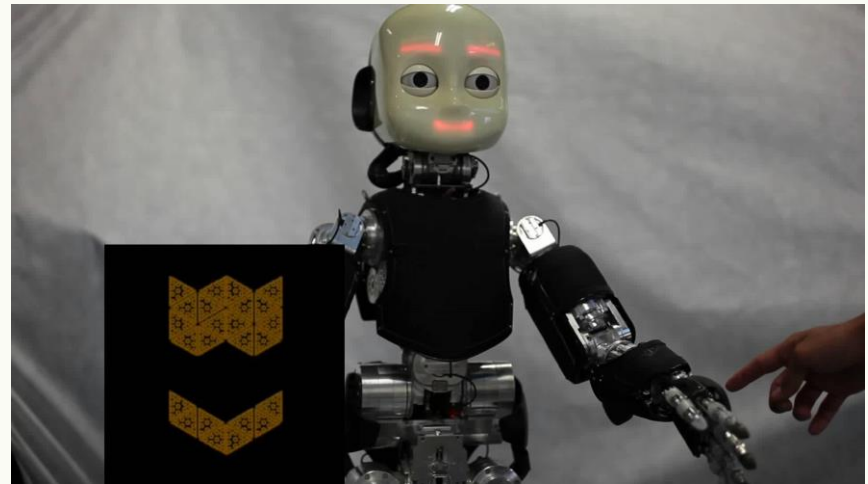
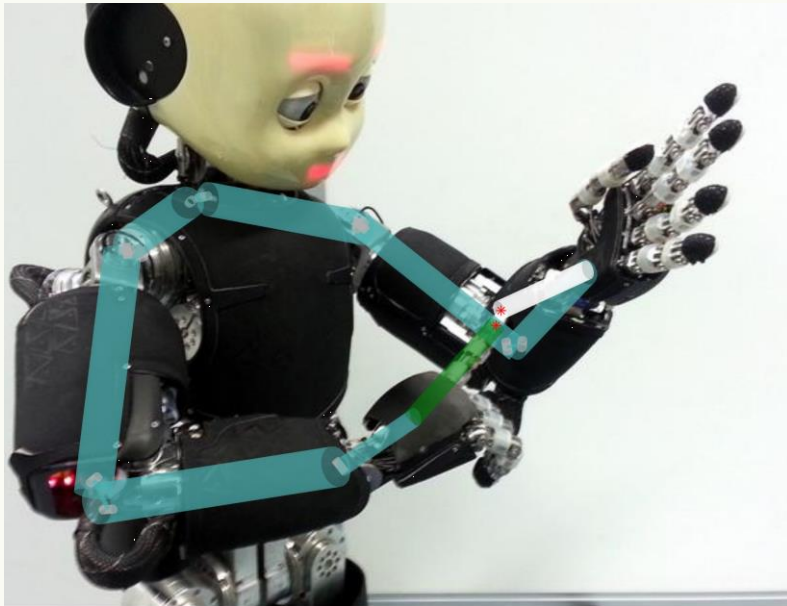
Rozlivek, J.; Rustler, L.; Stepanova, K. & Hoffmann, M. (2021), Multisensorial robot calibration framework and toolbox, in 'Humanoid Robots (Humanoids), IEEE-RAS International Conference on'.



Stepanova, K.; Rozlivek, J.; Puciov, F.; Krsek, P.; Pajdla, T. & Hoffmann, M. (2022), 'Automatic self-contained calibration of an industrial dual-arm robot with cameras using self-contact, planar constraints, and self-observation', *Robotics and Computer-Integrated Manufacturing*.

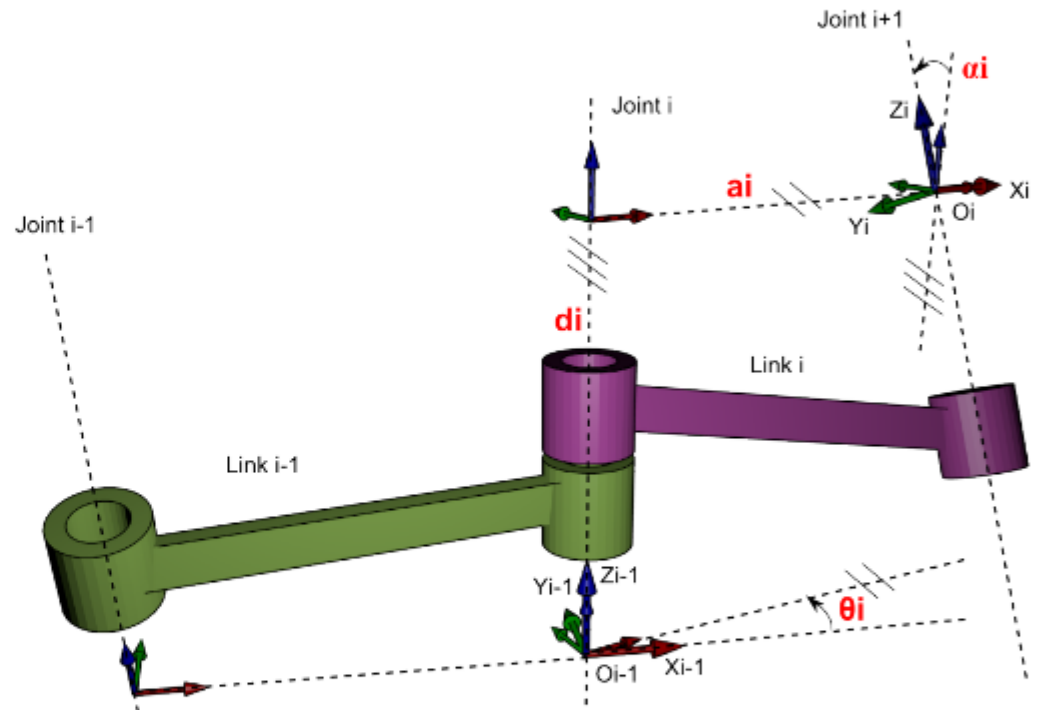
Self-contact to calibrate kinematics

- Using skin spatial calibration to fine-tune robot kinematics



Roncone, A.; Hoffmann, M.; Pattacini, U. & Metta, G. (2014), Automatic kinematic chain calibration using artificial skin: self-touch in the iCub humanoid robot, *in* 'Proc. IEEE Int. Conf. Robotics and Automation (ICRA)'.

Kinematic chain representation



■ Denavit-Hartenberg parameters [Wikipedia]

- d : offset along previous z to the common normal
- θ : angle about previous z , from old x to new x
- r : length of the common normal (aka a). Assuming a revolute joint, this is the radius about previous z .
- α : angle about common normal, from old z axis to new z axis

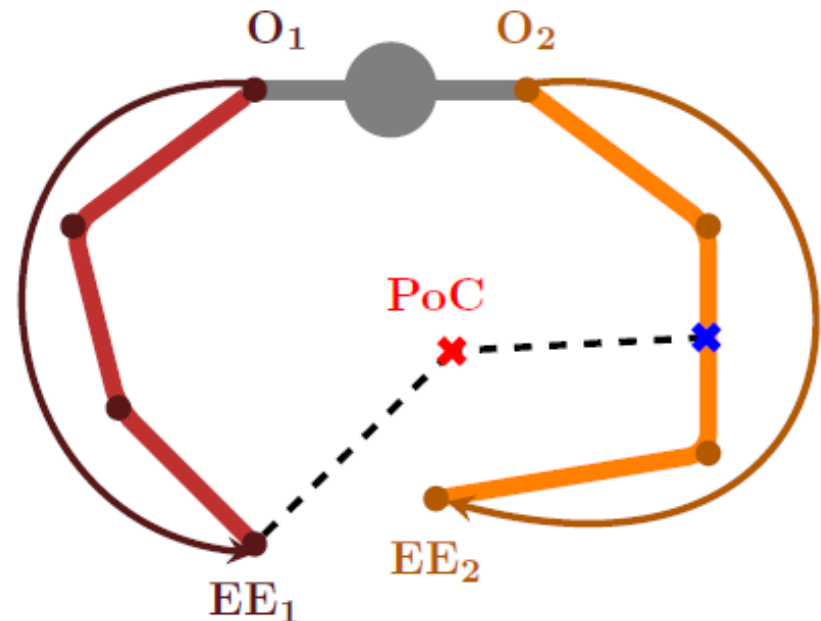
Making the robot touch its own body

Two fixed-base kinematic chains, with

- origins O_1 and O_2 (shoulders of iCub)
- end-effectors EE_1 and EE_2 (palms of the robot)
- blue cross – point to be touched
- PoC – final, *unknown*, point of contact in operational space

Problems:

- Limited nr. DOF for the task
- Finding PoC
- Undesired self-collisions at other points

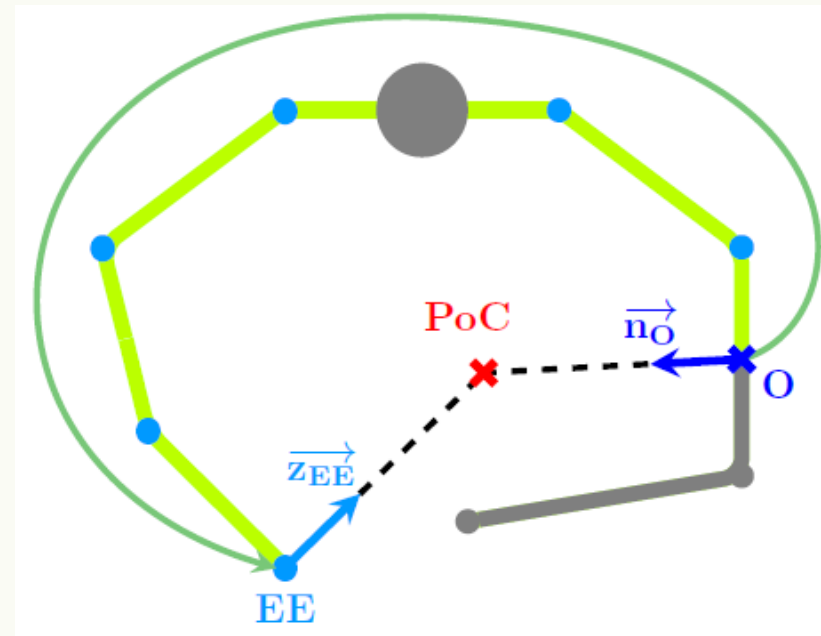


Reformulation of the kinematic chain

- > single floating-base serial chain with origin O in the point to be touched
 - half of the kinematic chain needs to be “reversed” – traversed upside down

Advantages:

- Final PoC defined *implicitly* (base is floating)
- More DOF available



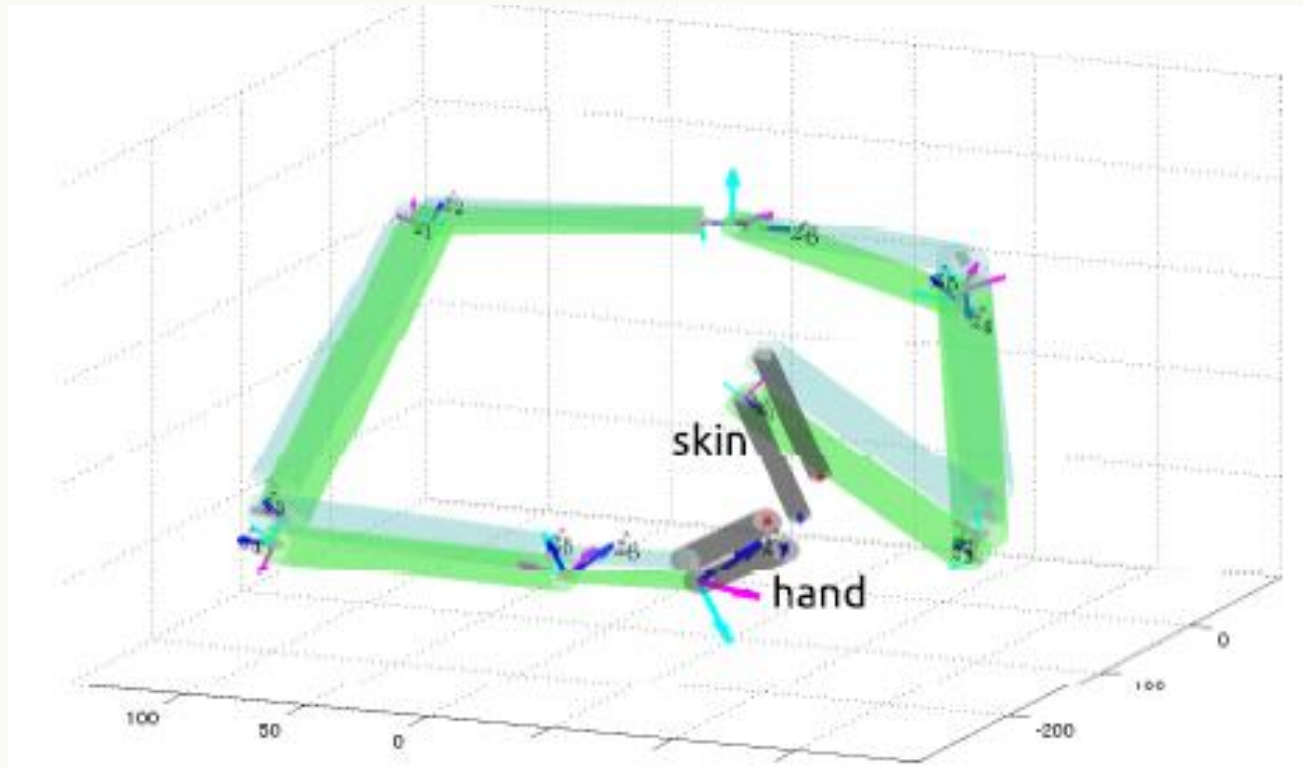
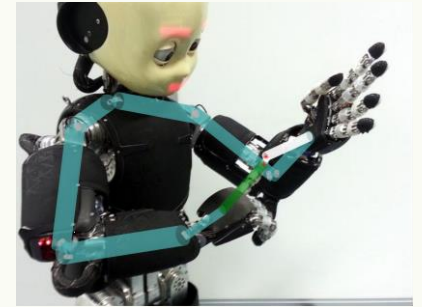
Self-calibration optimization problem formulation

Optimizing the parameter vector:

$\varphi_i = a_i, d_i, \alpha_i, o_i$ with $i \in [1, n]$,

- where $a, d, \alpha,$ and o are the Denavit-Hartenberg parameters
- in our case $n=12$, i.e. 12 DoF (5 on the «touched» and 7 on «touching» arm)

Optimization problem formulation (2)



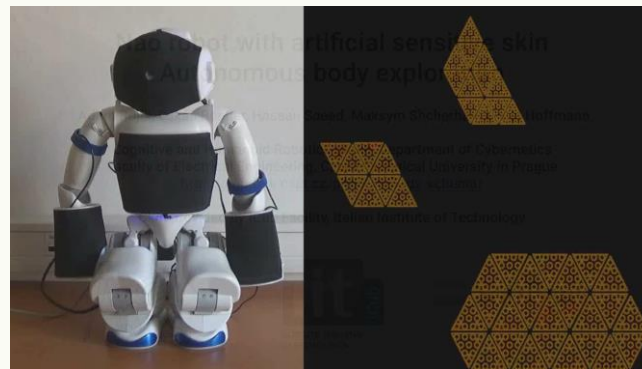
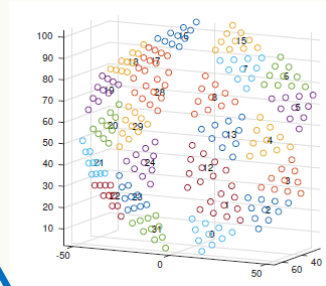
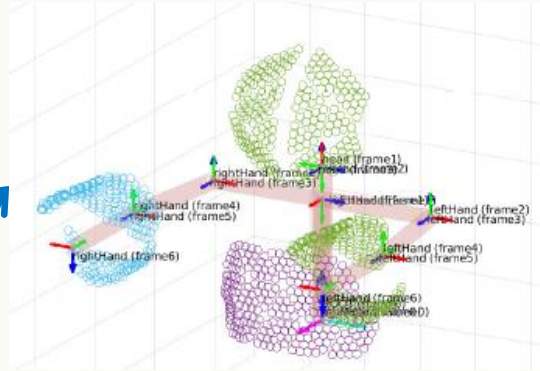
Optimization problem formulation (3)

$$\Phi^* = \mathit{arg} \min_{\Phi} \sum_{m=1}^M \|\mathbf{p}_s - \mathbf{p}_e(\Phi, \theta_m)\|$$

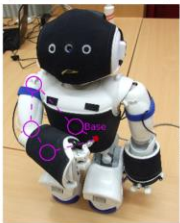
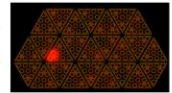
- Minimizing total position error, where
 - θ_m are joint angles of m-th sample as read from joint encoders
 - \mathbf{p}_e is the estimated position as a function of joint angles and current param. values
 - \mathbf{p}_s of the end-effector as measured from the skin

Self-contact to calibrate skin

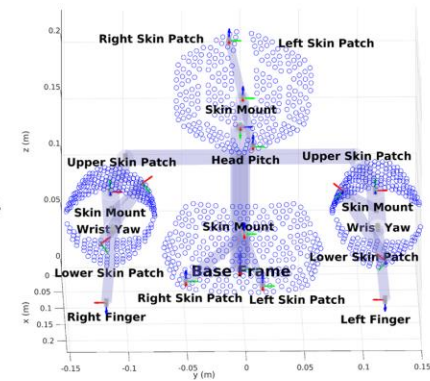
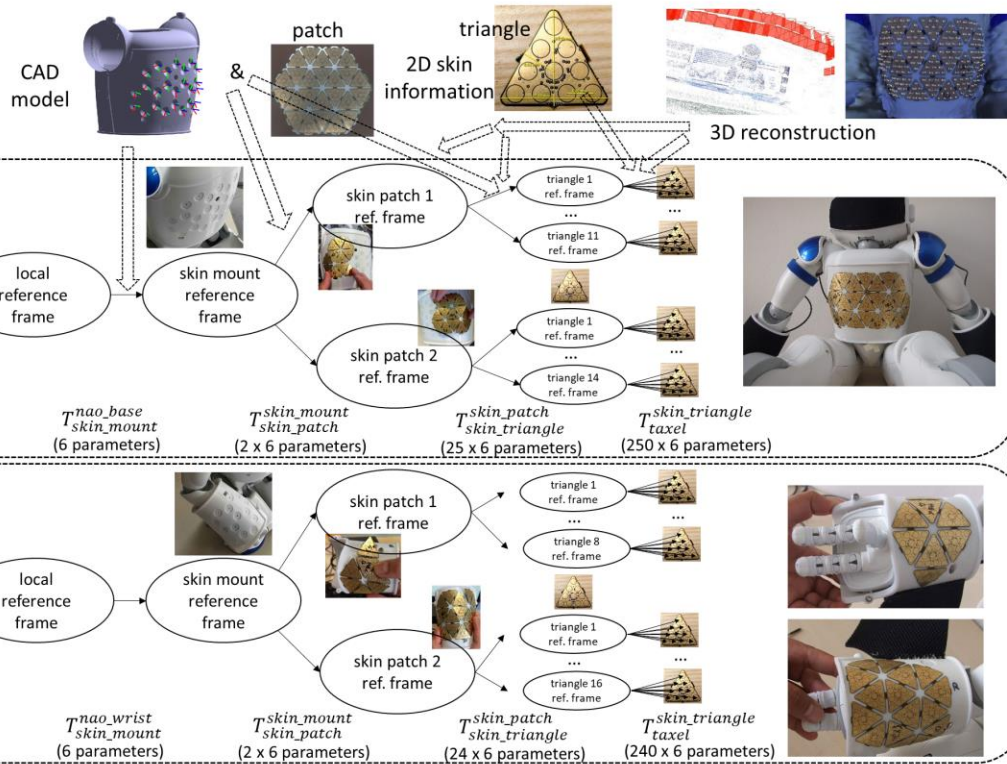
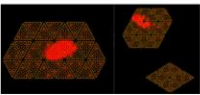
- Using kinematics for skin spatial calibration



self-contact with finger
(3 parameters for finger)



self-contact skin-on-skin



Rustler, L.; Potocna, B.; Polic, M.; Stepanova, K. & Hoffmann, M. (2021), Spatial calibration of whole-body artificial skin on a humanoid robot: comparing self-contact, 3D reconstruction, and CAD-based calibration, in 'Humanoid Robots (Humanoids), IEEE-RAS International Conference on', pp. 445-452.

Self-observation to calibrate kinematics

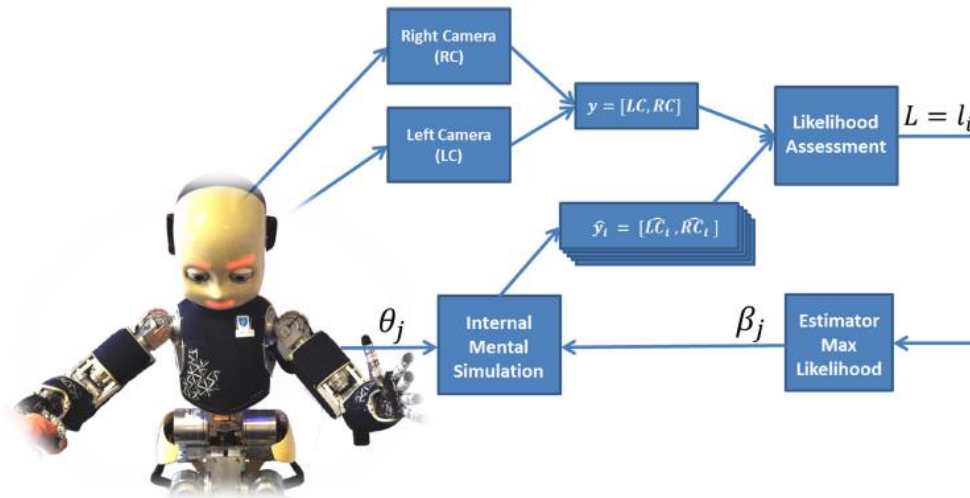


FIGURE 1 | The iCub humanoid robot uses its internal mental simulation to imagine (generate synthetic images of) the hand pose in real time. By comparing the generated images (\hat{y}_i) to the ones obtained through stereo vision (y), it simultaneously achieves better hand pose estimation and automatic calibration of the internal model.

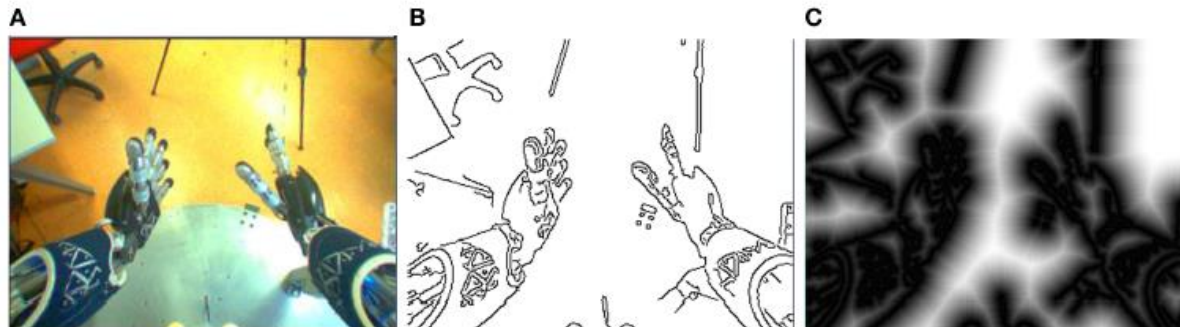
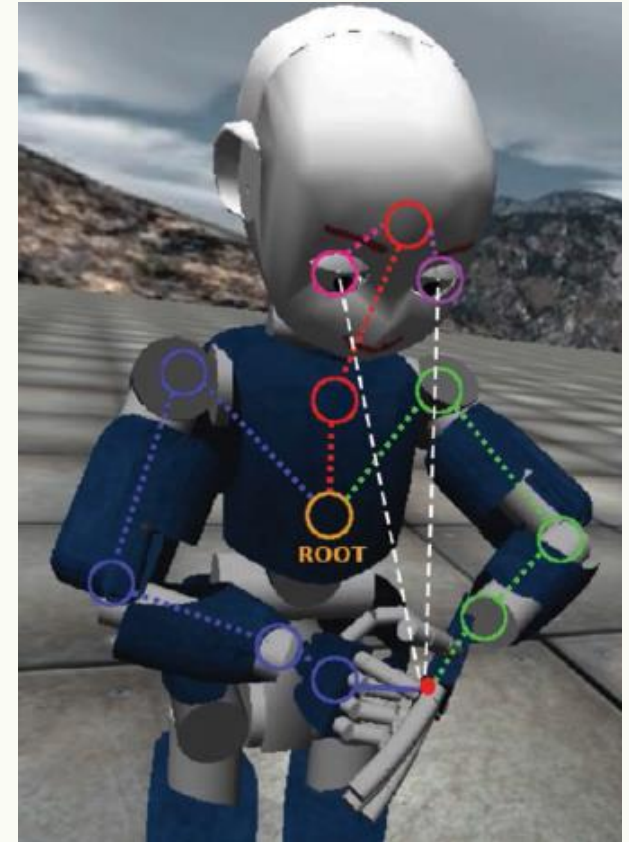
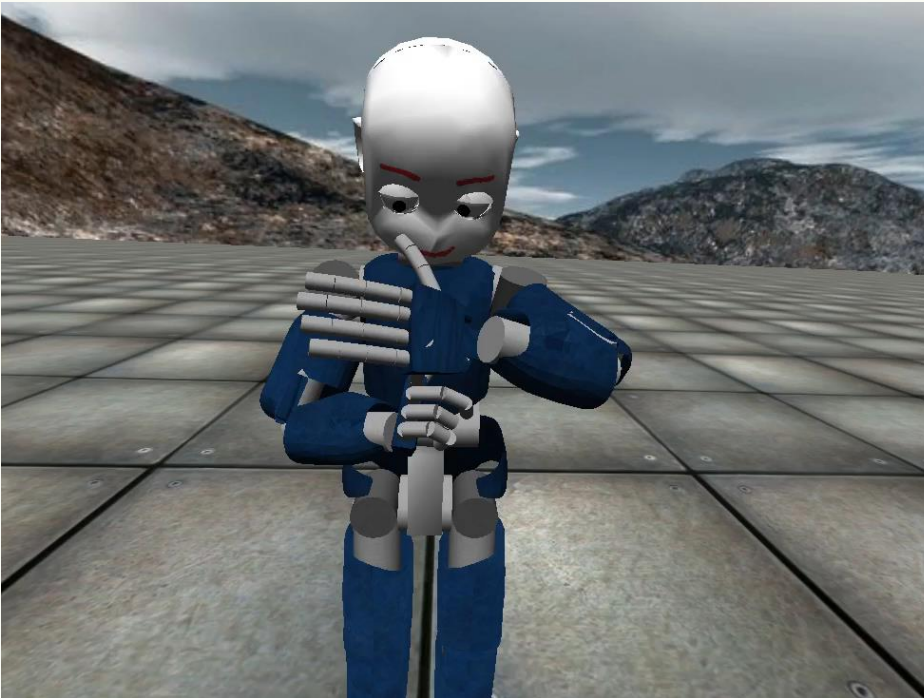


FIGURE 5 | Example of the computation of the edges and distance transform of the iCub hand in a real environment on the right camera. (A similar example can be shown for the left camera.) (A) is the input image, (B) shows the edges extraction using Canny, 1986, and (C) the distance transform using Borgefors, 1986.

Multi-chain calibration

- Multiple kinematic chain closures
 - Self-touch
 - Self-observation (vision)



Stepanova, K.; Pajdla, T. & Hoffmann, M. (2019), 'Robot self-calibration using multiple kinematic chains – a simulation study on the iCub humanoid robot', *IEEE Robotics and Automation Letters* 4(2), 1900-1907.

Multi-chain optimization function

TABLE I
DH PARAMETERS (a, d, α AND OFFSETS o) DESCRIBING ALL LINKS IN LEFT
ARM KINEMATIC CHAIN

Link(i)	a(i) [mm]	d(i) [mm]	α [rad]	o [rad]
1	23.36	143.3	$\pi/2$	$105 * \pi/180$
2	0	107.74	$-\pi/2$	$\pi/2$
3	0	0	$\pi/2$	$-\pi/2$
4	15	152.28	$-\pi/2$	$75 * \pi/180$
5	-15	0	$\pi/2$	0
6	0	137.3	$\pi/2$	$-\pi/2$
7	0	0	$\pi/2$	$\pi/2$
8	62.5	-16	0	0

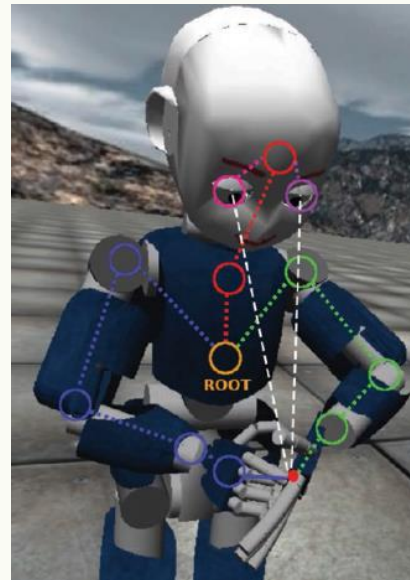
TABLE II
DH PARAMETERS – LEFT EYE KINEMATIC CHAIN

Link(i)	a(i) [mm]	d(i) [mm]	α [rad]	o [rad]
1	2.31	-193.3	$-\pi/2$	$\pi/4$
2	33	0	$\pi/2$	$\pi/4$
3	0	1	$-\pi/2$	$\pi/4$
4	-54	82.5	$-\pi/2$	$\pi/4$
5	0	-34	$-\pi/2$	0
6	0	0	$\pi/2$	$-\pi/4$

TABLE III
DH PARAMETERS – RIGHT EYE KINEMATIC CHAIN. LINKS 1–4 SHARED WITH
LEFT EYE KINEMATIC CHAIN

Link(i)	a(i) [mm]	d(i) [mm]	α [rad]	o [rad]
5	0	34	$\pi/2$	$-\pi/4$
6	0	0	$-\pi/2$	0

$$\begin{aligned} \phi^* = \operatorname{argmin}_{\phi} \sum_{m=1} \{ & \mu \cdot \| \mathbf{X}_m^{r,R}(\phi^r, \Theta_m^r) - \mathbf{X}_m^{l,R}(\phi^l, \Theta_m^l) \| \\ & + \| \mathbf{X}_m^{lL,I}(\phi^l, \phi^{le}) - \mathbf{u}_m^{lL} \| + \| \mathbf{X}_m^{rL,I}(\phi^r, \phi^{le}) - \mathbf{u}_m^{rL} \| \\ & + \| \mathbf{X}_m^{lR,I}(\phi^l, \phi^{re}) - \mathbf{u}_m^{lR} \| + \| \mathbf{X}_m^{rR,I}(\phi^r, \phi^{re}) - \mathbf{u}_m^{rR} \| \}^2, \end{aligned}$$



“Industrial humanoid”

- 1) Geometric kinematic calibration using **self-contained approaches** X calibration based on an external laser tracker
- 2) How the individual methods can be combined into a **single cost function**
- 3) Simultaneous (all parameters at once) X sequential calibration
- 4) New **dataset** for robot kinematic calibration

Calibrated parameters

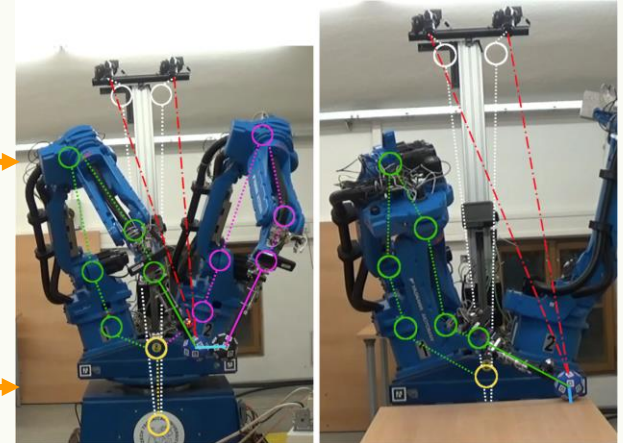
- custom end effector
- joint offsets of the complete kinematic chain of one arm
- full Denavit-Hartenberg (DH) representation of the platform

Setup

2 industrial manipulators, a common base, force/torque sensors at wrists, 2 cameras, special end effectors with fiducial markers

Calibration methods

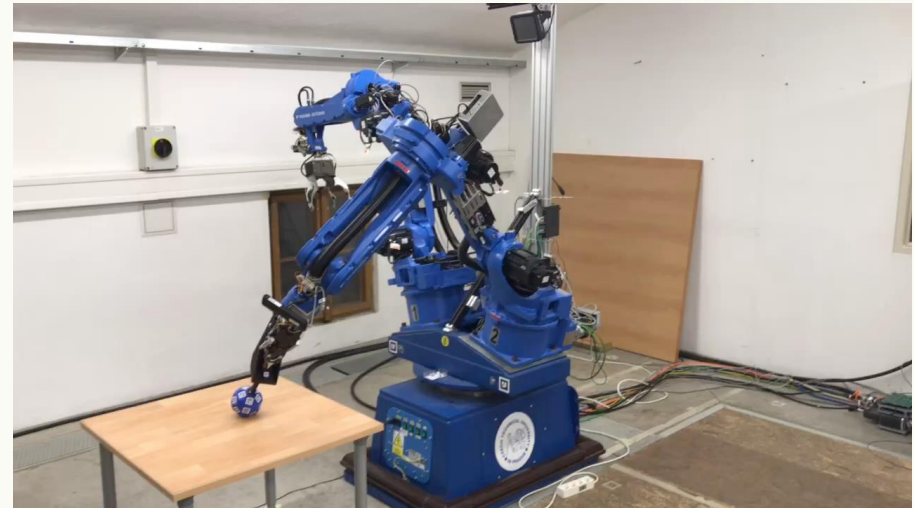
self-contact, planar constraints, self-observation, laser tracker



Stepanova, K.; Rozlivek, J.; Puciow, F.; Krsek, P.; Pajdla, T. & Hoffmann, M. (2022), 'Automatic self-contained calibration of an industrial dual-arm robot with cameras using self-contact, planar constraints, and self-observation', *Robotics and Computer-Integrated Manufacturing* **73**, 102250. [[DOI](#)][[Elsevier - OPEN ACCESS pdf](#)][[youtube-video](#)]

Multi-chain calibration

- Multiple kinematic chain closures
 - Self-touch
 - Self-observation (vision)
- Contact with a planar constraint



Stepanova, K.; Rozlivek, J.; Puciov, F.; Krsek, P.; Pajdla, T. & Hoffmann, M. (2022), 'Automatic self-contained calibration of an industrial dual-arm robot with cameras using self-contact, planar constraints, and self-observation', *Robotics and Computer-Integrated Manufacturing* **73**, 102250. [[DOI](#)][[Elsevier - OPEN ACCESS pdf](#)][[youtube-video](#)]

4.4. Combining multiple chains (LA-RA-LEye, LA-RA-LEye-REye)

In order to estimate all kinematic parameters of the robot, we can take advantage of combining some or all of the above-mentioned kinematic chains. For example, in the case that we combine LA-RA, LA-LEye and LA-REye chains together into LA-RA-LREye (see Fig. 14), the estimated parameter vector ϕ consists of the following parameters: $\phi = \{\phi^r, \phi^l, \phi^{rc}, \phi^{lc}\}$, where ϕ^l , ϕ^r , ϕ^{rc} , and ϕ^{lc} are parameters corresponding to the left arm, right arm, right camera, and left camera, respectively. Similarly, contact of right arm with a horizontal and vertical plane can be combined with self-observation by right camera, resulting in the parameter vector ϕ : $\phi = \{\phi^r, \phi^{rc}, n^{hp}, d^{hp}, n^{vp}, d^{vp}\}$, where n^{hp} and d^{hp} are parameters defining the horizontal plane, and n^{vp} and d^{vp} are parameters defining the vertical plane.

The overall objective function can be generally defined as (depending on which datasets and criteria we want to use for calibration):

$$g(\phi, D, \zeta) = [k^{st} \odot g^{st}(\phi, D^{st}, \zeta), k^p \odot g^p(\phi, D^p, \zeta), k^{so} \odot g^{so}(\phi, D^{so}, \zeta)], \quad (15)$$

where D^{st} , $D^p = \{D^{hp1}, D^{hp2}, D^{vp}\}$ and $D^{so} = \{D^{st}, D^p\}$ are datasets for self-touch, planar constraints optimization, and self-observation, respectively. Parameters k^{st}, k^p, k^{so} are scale factors to reflect the different uncertainty/reliability of the components, the number of measurements per configuration, and transformations from distance errors given in meters with the reprojection errors in pixels. Symbol \odot marks a Hadamard product: i.e. $(k^{st} \odot g^{st})_i = k_i^{st} \cdot g_i^{st}$. The value of these parameters is set independently for each pose: $k_i^{st} = \eta_i^{st} \cdot p^{st} \cdot \mu_i$, $k_i^p = \eta_i^p \cdot p \cdot \mu_i$, and $k_i^{so} = \eta_i^{so} \cdot p^{so}$, where $\eta^{st}, \eta^p, \eta^{so}$ reflect the reliability of the measurement (e.g., $\eta_i = \sigma_i^{-\frac{1}{2}}$, where σ_i is the uncertainty of the measurement in the given pose). In this work, $\eta = 1$ was used for all approaches. The parameter p_i reflects the fact that there are multiple markers detected by cameras for the given contact configuration. Therefore, in the case of (planar constraints/self-touch) contact and self-observation combination $p^p = 10$, $p^{st} = 20$ (there are two icosahedrons in contact and on average 20 marker detections per contact event), and $p^{so} = 1$. The coefficient μ_i is determined from intrinsic parameters of cameras (60 deg horizontal view angle, image size 4000×6000 px) and distance d_i of the end effector from the camera: $\mu_{i,x} = 4000\text{px}/(d_i(\pi/3))$, $\mu_{i,y} = 6000\text{px}/(d_i(\pi/3))$. For simplicity,

Stepanova, K.; Rozlivek, J.; Puciow, F.; Krsek, P.; Pajdla, T. & Hoffmann, M. (2022), 'Automatic self-contained calibration of an industrial dual-arm robot with cameras using self-contact, planar constraints, and self-observation', *Robotics and Computer-Integrated Manufacturing* **73**, 102250. [DOI][Elsevier - OPEN ACCESS pdf][youtube-video]

Resources

- Ch. 7 Sensors in Correll, N., Hayes, B., Heckman, C., Roncone, A. (2022). Introduction to Autonomous Robots: Mechanisms, Sensors, Actuators, and Algorithms, MIT Press (forthcoming). [FREELY AVAILABLE]. <https://github.com/Introduction-to-Autonomous-Robots/Introduction-to-Autonomous-Robots>
- Hoffmann, M. (2022), Biologically inspired robot body models and self-calibration, *in* Marcelo Ang; Oussama Khatib & Bruno Siciliano, ed., 'Encyclopedia of Robotics', Springer. [[DOI](#)]

Multisensorial robot calibration toolbox

<https://github.com/ctu-vras/multirobot-calibration>

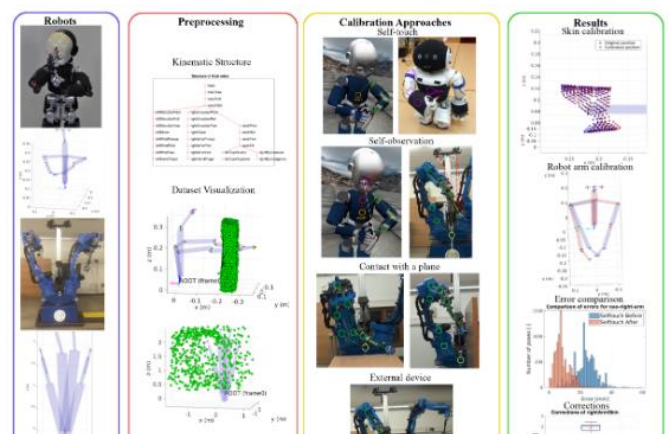
rustlluk Update README.md erassba on Dec 18, 2020 211 commits

File	Commit Message	Time
@Robot	copyright added	2 months ago
Calib	copyright added	2 months ago
Results	DH->kinematics, joint->link	2 months ago
UserData	DH->kinematics, joint->link	2 months ago
Utils	copyright added	2 months ago
Visualisation	copyright added	2 months ago
MRC.mlappinstall	copyright added	2 months ago
README.md	Update README.md	2 months ago
gui.mlapp	copyright added	2 months ago
overview.png	Smaller image	2 months ago
tasks.csv	Deleted other images, updated task.csv	2 months ago

README.md

Multisensorial robot calibration framework and toolbox

This toolbox provides a solution to the multi-chain calibration of a general robot by combining multiple calibration approaches. Users can define an arbitrary robot, choose calibration approach, set parameters of the optimization solver and the calibration. The results can be saved for later use and evaluated with a variety of prepared visualizations. Also, a user-friendly GUI is available, which makes the calibration of robots accessible even for the general public.



The screenshot displays the README.md content for the 'Multirobot Calibration' toolbox. It is organized into four main columns:

- Robots:** Shows images of different robot models and their kinematic structures.
- Preprocessing:** Includes 'Kinematic Structure' diagrams, 'Dataset Visualization' plots, and 'External device' images.
- Calibration Approaches:** Features 'Self-observ.' and 'Self-observatory' images, 'Contact with a plane' diagrams, and 'External device' images.
- Results:** Contains 'S&M calibration' plots, 'Robot arm calibration' plots, 'Error comparison' histograms, and 'Corrections' plots.

Rozlivek, J.; Rustler, L.; Stepanova, K. & Hoffmann, M. (2021), Multisensorial robot calibration framework and toolbox, *in* 'Humanoid Robots (Humanoids), IEEE-RAS International Conference on'.